Advances in Geo-Energy Research

Vol. 4, No. 3, p. 233-246, 2020

Original article

The application of improved differential evolution algorithm in electromagnetic fracture monitoring

Ji Qi[1], Liming Zhang[1], Kai Zhang[1]*, Lixin Li[2], Jijia Sun[1]

[1]*School of Petroleum Engineering, China University of Petroleum (East China), Qingdao 266580, P. R. China*

[2]*PetroChina Richfit Information Technology Co., Ltd, Beijing 100000, P. R. China*

Keywords:
Electromagnetic monitoring
hydraulic fracture
conductive proppant
inversion
differential evolutionary algorithm

Cited as:
Qi, J., Zhang, L., Zhang, K., Li, L., Sun, J. The application of improved differential evolution algorithm in electromagnetic fracture monitoring. *Advances in Geo-Energy Research*, 2020, 4(3): 233-246, doi: 10.46690/ager.2020.03.02.

Abstract:
Hydraulic fracturing is a pivotal technology in the development of unconventional tight reservoirs, in which accurate monitoring of fracture parameters is significant. This paper proposes an improved differential evolution algorithm (EMDE) to calculate the Effective Propped Volume (EPV) accurately. The forward simulation results demonstrate that when the transmitting source plane is in a particular position, the relationship between signals and a specific parameter is the most obvious, providing a basis for the application of inversion algorithms. Furthermore, the difference between the population center and the individual is added to accelerate the convergence of the EMDE algorithm. A simplified selection strategy of the simulated annealing algorithm is used to enhance the convergence speed and the ability to find the global optimal value of the objective function simultaneously. The one-stage and two-stages inversion strategies are designed to calculate the parameters. In the two-stage inversion, the second-stage is constrained by the forward simulation and the first-stage results. It indicates that the errors of the two-stages inversion can be controlled within 5%. Through the inversion simulation proposed in this paper, the feasibility of the electromagnetic method to monitor the EPV is verified, and it provides a theoretical guidance for subsequent fracturing construction adjustments.

1. Introduction

Unconventional oil and gas resources have the characteristics of wide distribution and large reserves, which is a significant candidate for future energy development. Hydraulic fracturing is an essential stimulation approach to increase the production of unconventional reservoirs. In the process of hydraulic fracturing and subsequent development, accurate measurement of fracture morphology and volume can provide crucial guidance for subsequent well pattern design, refracturing, the fracturing of new wells, and production scheme design.

At present, microseismic mapping, clinometer, and downhole tiltmeter mapping are widely used measurement methods. However, some limitations still exist in these methods such as the lack of ability to monitor fracture width or conductivity (Basu and Sharma, 2014). Therefore, a cheap, direct, accurate strategy to measure the morphology of hydraulic fractures, especially the Effective Propped Volume (EPV) is required.

The idea of using electromagnetic theory for fracture monitoring has drawn attentions. Symington et al. (2010) proposed an electro fracture method to convert shale oil and gas to producible. It used a conductor with appropriate electrical resistivity to heat formations in-situ. LaBrecque et al. (2016) put detection points on the surface and conducted a small range of field experiments using the electromagnetic monitoring method to measure the volume of the fracture. Palisch et al. (2016) conducted a far-field experiment, a neo-proppant used for electromagnetic monitoring was tested. They conducted a far-field experiment, in which a neo-proppant used for electromagnetic monitoring was tested. Cipolla et al. (2009) cooperated with Carbo Company conducted a simulation to study the influence of proppant distribution on production. Basu et al. (2014) used low-frequency electromagnetic induction to diagnose fracture geometry, cases of fractures, wellbore in different relative locations, and the proppant distribution impact on the monitoring signals.

In the subsequent processing of received signals, appropri-

Yandy Scientific Press

*Corresponding author.
E-mail address: q515974340@163.com (J. Qi); zhangliming@upc.edu.cn (L. Zhang); zhangkai@upc.edu.cn (K. Zhang); llxxll_2011@163.com (X. Li); s19020147@s.upc.edu.cn (J. Sun).

Received April 27, 2020; revised May 29, 2020; accepted May 31, 2020; available online June 7, 2020.

ate algorithms must be used to calculate the proper fracture parameters. The inversion methods for cross-well electromagnetic tomography (Newman and Alumbaugh, 1997; Liu et al., 2008) and 3-D imaging from a single wellbore (Alumbaugh, 2001; Mallan and Alumbaugh, 2004; Abubakar and Habashy, 2006) have become increasingly complete.

Scholars have studied various inversion algorithms for different specific problems. In the wellbore-surface 3-D data inversion, the approximate iterative method reduces the large data amount of computation and storage, but due to the low accuracy, the inversion results are limited to qualitative or semi-quantitative interpretations. In recent years, based on the complete solution of the nonlinear inversion methods are proposed, the accuracy of the inversion is promoted without too much computation. Abubakar et al. (2008) developed a Gauss-Newton regularization inversion method. The inversion of cross-well electromagnetic field used the multiple optimization objective functions combining with the least square method. The model and radial basis function were used to invert the surface-wellbore electromagnetic data (Li et al., 2011). Although the inversion speed and stability were increased, the inversion process relied heavily on the constraint conditions and the initial model. Nonlinear conjugate gradient method was popular for wellhead electromagnetic data inversion. Wang et al. (2011) used a reweighted regularized conjugate gradient method for wellhead electromagnetic data inversion. Zhang et al. (2011) explored the application of the nonlinear conjugate gradient method to invert the borehole-surface magnetotelluric data. The research of nonlinear conjugate gradient inversion method in the wellbore electromagnetic field was at the primary stage of development. Its inversion iteration process did not depend on the selection of initial value, program implementation was simple, and it could obtain the global optima convergence. Further, the dimensionality of the simulation problem usually had no effect on the rate of convergence in this strategy, so the problem of high-dimensional inversion could be solved effectively.

Different from other wellbores electromagnetic data inversions, the electromagnetic observation signal in this paper is obtained by the monitoring instrument moving and scanning in the wellbore, providing constraints for the inversion algorithm according to the simulated forward results. In the accurate simulation, the peak signal section presents different characteristics. The primary purpose of the inversion algorithm is to correct the fracture azimuth, length, and height by fitting the peak area data of the observation signal. The least-square method can be applied to the solution process. However, it has some drawbacks due to the non-convergence problems caused by the partial derivatives solution (Ruan, 1999). In recent studies, the differential evolution (DE) algorithm has been widely used in the inversion of electromagnetic wave signals due to its simplicity, improvable character, and high adaptability, which will be described specifically in following sessions.

Section 2 presents the mathematical and physical models, the sensitivity analysis, the forward results. Section 3 gives the inverse method. The inversion examples and results are presented in section 4.

2. Forward modeling method for electromagnetic monitoring of propping fractures

For the application of Electromagnetic (EM) technology in the fracture monitoring, conductive proppant will be used instead of traditional proppant to generate conductive fractures. It will increase the conductive contrast between the fracture and the background matrix. Subsequently, the electromagnetic signal transmitter is employed to move along the wellbore and transmit signals to generate a primary electromagnetic field. The conductive fractures respond to the primary electromagnetic field and generate the secondary electromagnetic field. The receiving tool records the corresponding field strength and direction of the primary and secondary electromagnetic field. Therefore, the fracture volume calculated by this method is the EPV, rather than Stimulated Reservoir Volume (SRV).

The main objective of the forward simulation is to change each parameter solely. When the transmitting source plane and the coordinate axis are at different angles, the forward simulation obtain the received signals through numerical simulation, analyze the difference of the received signals, determine the parameter corresponding to the signals with the maximum difference, and provide constraints for the subsequent inversion algorithm.

2.1 Mathematical and Physical modeling

Fig. 1 illustrates a schematic diagram of the horizontal well and fractures. The horizontal well extends along the Z direction. The fracture plane is within the XY plane or at a certain azimuth with the XY plane. The model assumes that the diameter of the wellbore is 0.2 m, and the hydraulic fracture extends outward centered from the wellbore's outer diameter. This paper simulates an open hole well which assumes thatthe electrical characteristics of background space (reservoir) are homogeneous.

Due to the high computational complexity of the 3-D model, a reduced model is established. The geometry of the fracture is rectangular, of which the length and height are less than 20 m. The thickness is set as 0.2 m, and the reservoir is a cube model of 100 m $\times$ 50 m $\times$ 50 m. The electrical param-

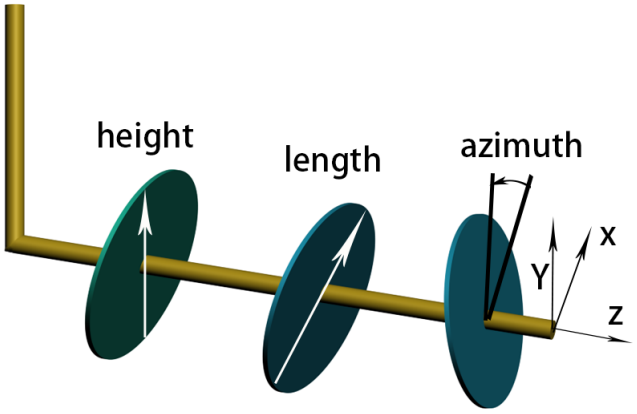

Fig. 1. Schematic diagram of the wellbore and fracture parameters.

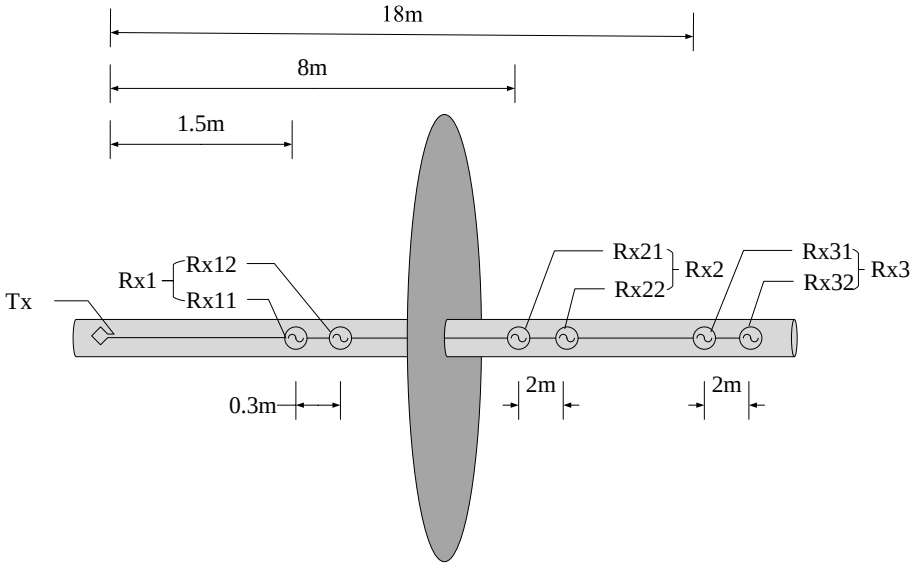

Fig. 2. Schematic of triaxial transmitting Tx- triaxial receiving Rx instrument.

eters, including conductivity and permeability of the reservoir, are known. In practical applications, these parameters are measured before signal processing by field engineers.

The model consists of electromagnetic anomalous bodies, i.e. the fracture filled by the electromagnetic proppant, the wellbore, the monitoring tools and the reservoir. The fracture is assumed to be uniformly filled with proppant; hence, the fracture conductivity is assumed to be homogeneous, and the boundary layer of the model is assumed to be a perfect electrical conductor, i.e.:

$$n \times E = 0 \tag{1}$$

The constitutive equation of electromagnetic wave propagation is Maxwell's equations. It assumes that a current source J produces an electric field E and a magnetic field H in the three-dimensional domain $\Omega \subset R^3$. J, E, H are all three-dimensional and complex number vector fields. Maxwell's equation describes the relations between these fields by characterizing the constitutive properties of the medium:

$$\nabla \times H = (\sigma - i\omega\varepsilon)E + J \tag{2}$$

$$\nabla \times E = i\omega\mu H \tag{3}$$

$$\nabla \times \varepsilon E = \rho_T \tag{4}$$

$$\nabla \times \mu H = 0 \tag{5}$$

where σ is the conductivity; ε is the dielectric constant; μ is the permeability; σE is the inductive reactance current; $-i\omega\varepsilon E$ is the inductive displacement current; J is the impressed current; ρ_T is the total charge density in the definitional domain.

The difference equation of Eq. (2) is formulate as:

$$i\omega\rho_T = \nabla \cdot (J + \sigma E) \tag{6}$$

So ρ_T comes from the sum of the difference of J and $\nabla \cdot \sigma E$. The charge is taken at the discontinuity of σE, and the cumulative charge is going to be applied to ρ_T. Only in the special case of $\sigma = 0$ can we know the initial value of ρ_T. This is rare in geophysical problems (essentially only within the resistance tool), so ρ_T is not considered in the model.

When the impressed current is DC, $\omega = 0$, maxwell's equations applied to this simulation can be simplified as follows:

$$\nabla \times H = \sigma E + J \tag{7}$$

$$\nabla \times E = 0 \tag{8}$$

$$\nabla \times \mu H = 0 \tag{9}$$

In Eq. (7), J is the impressed current, that is, the electromagnetic transmission source in the model, which can be either non-scattered field or scattered field.

2.2 Monitoring tools for modeling

In Fig. 2, Tx represents the three-axis transmitter, Rx1, Rx2, Rx3 are three receiving points. Each receiving point contains two receivers: Rx11, Rx12, Rx21, Rx22, Rx31, Rx32. The transmitter Tx contains three toroidal coils. Each toroidal coil plane is perpendicular to the X-axis, Y-axis, Z-axis, respectively, Tx can be adjusted to be perpendicular to the M-axis (M-axis is formed when the Z-axis rotates anticlockwise 45 degrees in the XZ plane.) if necessary.

In the actual cases, the monitoring instrument moves and scans along the wellbore, the fracture, while the reservoir

Table 1. The simulated parameters.

Parameters	Value	Parameters description
row_M	10000 [ohm·m]	Reservoir rock resistivity
row_F	0.001 [ohm·m]	Fracture resistivity
sigma_M	1/rou_M	Reservoir rock conductivity
sigma_F	1/rou_F	Anomalous body conductivity
Lx	50 [m]	The length of the model in the x-direction
Ly	50 [m]	The length of the model in the y-direction
Lz	100 [m]	Model z-direction length (shaft direction)
Thf	0.2 [m]	Thickness of fracture
ellipseA	12 [m]	Long semi-axis of fracture (length)
ellipseB	10 [m]	Short semi-axis of fracture (height)
AzimuthF	15 [deg]	Azimuth
Azimuth	0 [deg]	Azimuth of source surface

are stationary. In the model, the positions of transmitters and receivers are relatively static while the fracture is gradually moving along the wellbore. The purpose of setting up two receivers at each receiving point is to process two different signals by the linear method so as to eliminate the induced signals of the reservoir background field (Zhang et al., 2019)

In the simulation process, the initial position of the fracture is set as $z = -3.5$ m; the fracture moves in the positive direction of the Z-axis (wellbore axis direction), the scanning interval is 0.5 m. The specific parameters of the model are shown in the Table 1.

2.3 Sensitivity analysis

The signals obtained by receivers can be divided into four types: the real part of the electric field, the real part of the magnetic field, the imaginary part of the electric field, the imaginary part of the magnetic field. Through the whole simulation process, if all the four signals are collected and analyzed, it will undoubtedly increase the calculation amount. Therefore, we necessitate determining the most suitable type of signals through sensitivity analysis. Depending on the difference between the signal curves in each case, the signal type with the largest difference is considered to be the most sensitive to the current parameters.

(1) The existence of the fracture

Simulated conditions: Transmitting frequency is 100 Hz, the magnetic dipole moment of the toroidal coils is 100 A·m^2. Signals are received respectively when the fracture exists or not.

Simulated results: The imaginary part of the electric field and magnetic field signals are sensitive to the existence of fractures.

(2) Formation conductivity

Simulated conditions: Set the formation conductivity as 1E-2 S/m, 1E-3 S/m, 1E-4 S/m, 1E-5 S/m.

Simulated results: The real part of the electric field signals is the most sensitive to the deviation of the formation conductivity and the fracture location. The imaginary part of the magnetic field signals is sensitive to the location of the fracture.

(3) Transmitting frequency

Simulated conditions: Set the transmitting frequency as 1E+2 Hz, 1E+3 Hz, 1E+4 Hz, 1E+6 Hz.

Simulated results: The imaginary part of the magnetic field signals is the most sensitive to the deviation of the frequency and the location of the fracture.

In conclusion, though the real part of the electric field signals is the best to distinguish the formation conductivity and has the most significant strength, it can hardly distinguish the fracture locations in low-frequency transmitting, under which the sufficient detection range can be obtained (Huang and Boyle, 2008). Therefore, the imaginary part of the magnetic field signals is the most suitable to observe.

2.4 Forward simulation results

The pivotal parameters of the fracture are necessarily the length, the height, and the azimuth. They are the key parameters to determine the EPV. Previous simulation found that when the absolute values of azimuth are the same, the signals overlapped. Therefore, both the value and the sign should be taken into the calculation for the azimuth.

This method can be used to calculate the following five fracture parameters, according to them the three-dimensional morphology of simple fractures can be diagrammatized.

1) Transmitting frequency;
2) The height of the fracture;
3) Azimuth value;
4) Azimuth sign;
5) Multi-fracture system case.

The overall idea of forward-simulation is to set several groups of fracture parameters as single variable analysis, obtaining monitoring signals and the relationship between parameters and signals through simulation. The authors analyze all the signals, including signals from R×1, R×2, and R×3.

In the case of changing only one parameter and changing two parameters, Rx receives the signals when the transmitting source plane are perpendicular to the X-axis, the Y-axis, and the Z-axis. The listed figures represents results with the most apparent signal differences. In the legend of the attached figures, 'L' on behalf of the 'Length', 'H' for the 'Height', 'A' for the 'Azimuth', 'F1' for the 'first fracture', 'F2' for the 'second fracture'. The number after the letter is their value; the unit is 'm' for the length and height, '°' for the azimuth.

Figs. 3-8 illustrate the distributions of the signals in the forward simulation, when the transmitting source plane is in a specific position, the relationship between the signals and a specific parameter is the most obvious. When the transmitting source plane is perpendicular to the Z-axis, the peak area of the signals is sensitive to the length and height, the value of the azimuth is corresponding to the transmitting source plane perpendicular to the X-axis, the sign of the azimuth is corresponding to the transmitting source plane perpendicular to the M-axis. The forward simulation results provide constraints for the inversion process, especially the two-stages inversion and more accurate inversion results.

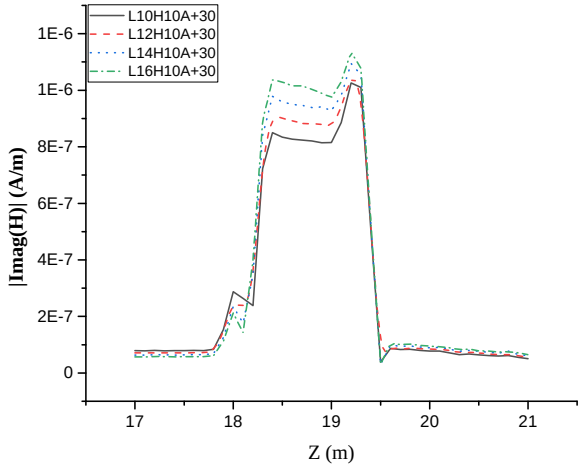

Fig. 3. The simulated results of fracture length (The transmitting source plane perpendicular to the Z-axis).

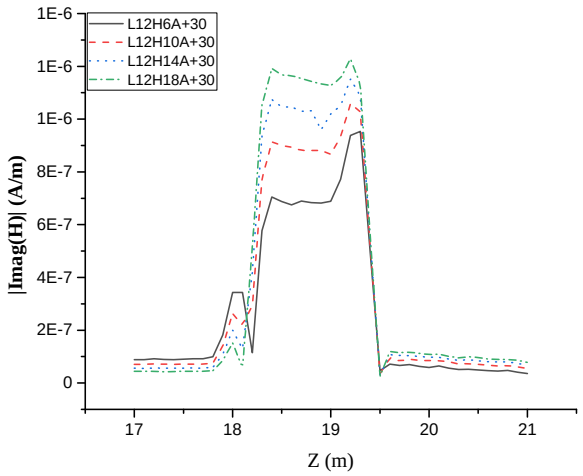

Fig. 4. The simulated results of fracture height (The transmitting source plane perpendicular to the Z-axis).

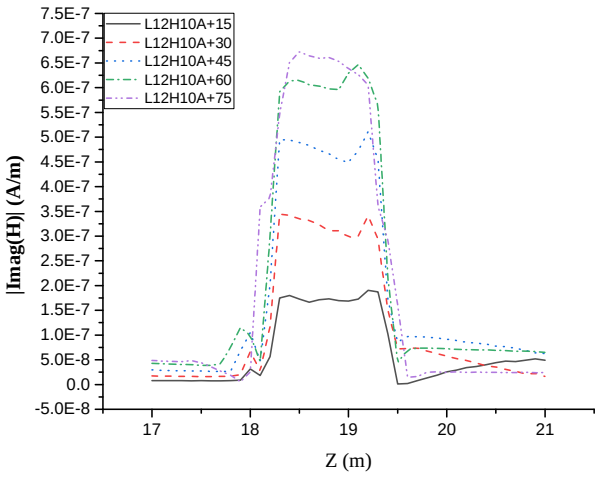

Fig. 5. The simulated results of azimuth value (The transmitting source plane perpendicular to the Z-axis).

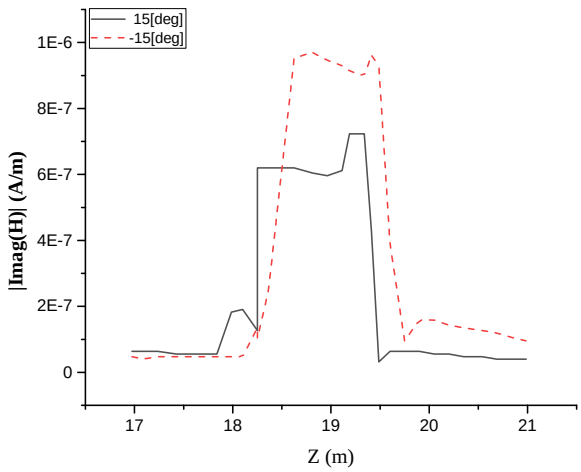

(a)

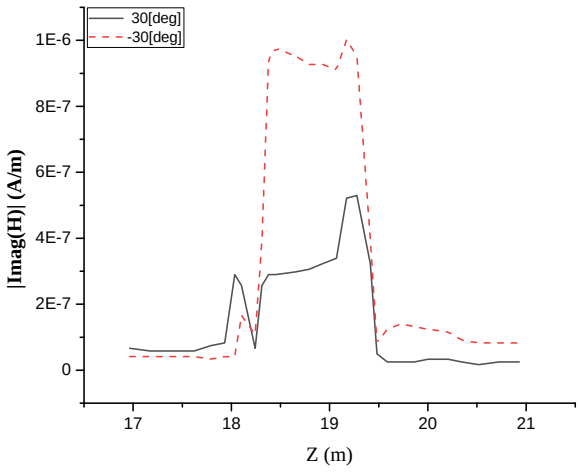

(b)

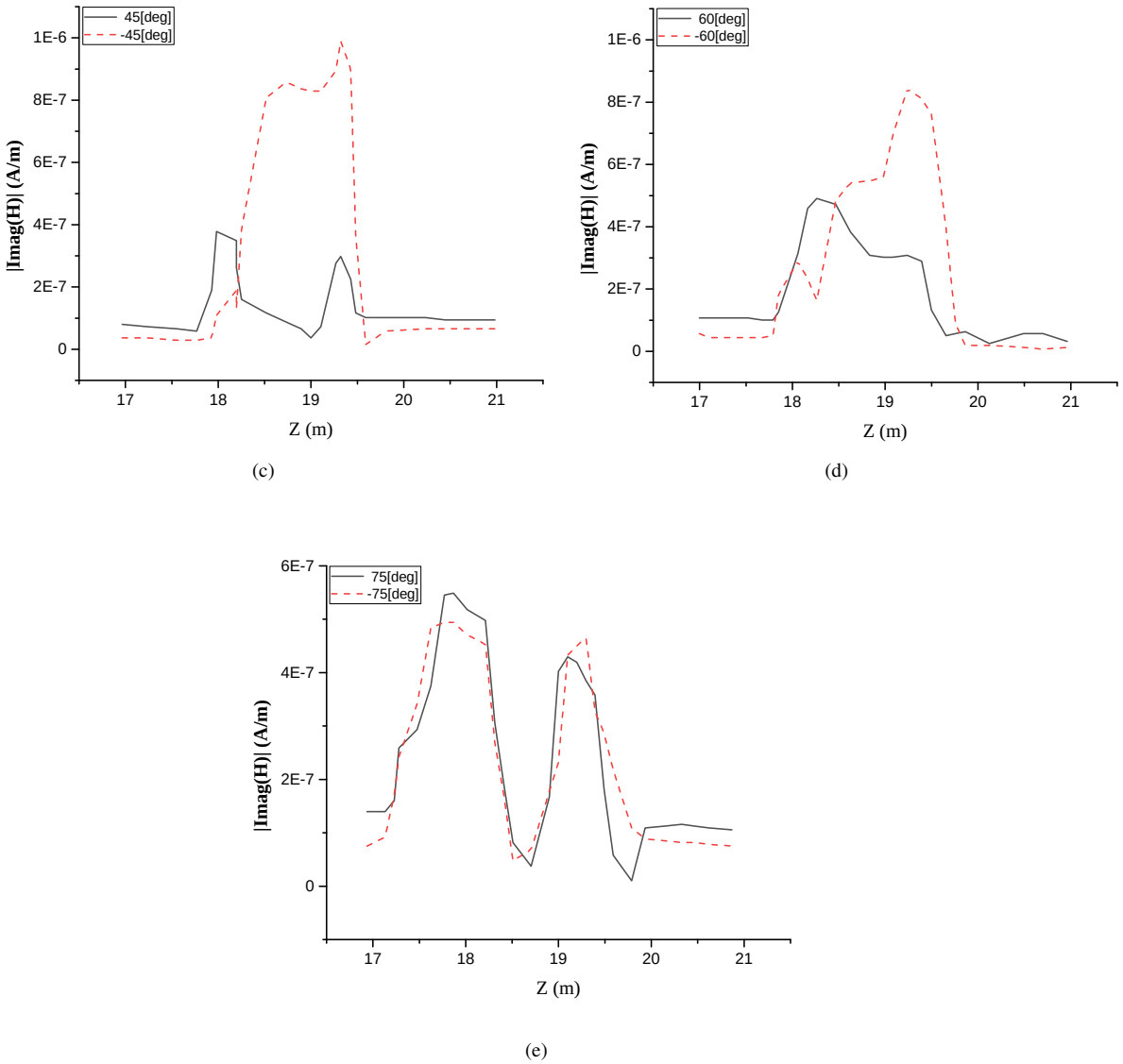

Fig. 6. The simulated results of azimuth sign (The transmitting source plane perpendicular to the M-axis). (a) +15 [deg] vs -15 [deg] (b) +30 [deg] vs -30 [deg] (c) +45 [deg] vs -45 [deg] (d) +60 [deg] vs -60 [deg] (e) +75 [deg] vs -75 [deg].

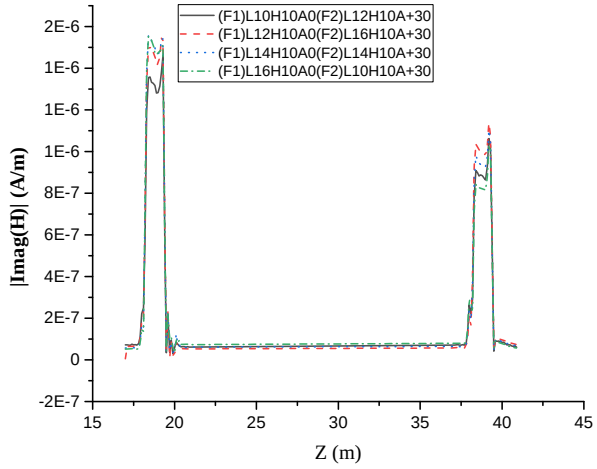

Fig. 7. The simulated results of multi-fracture system case with a constant height (The transmitting source plane perpendicular to the Z-axis).

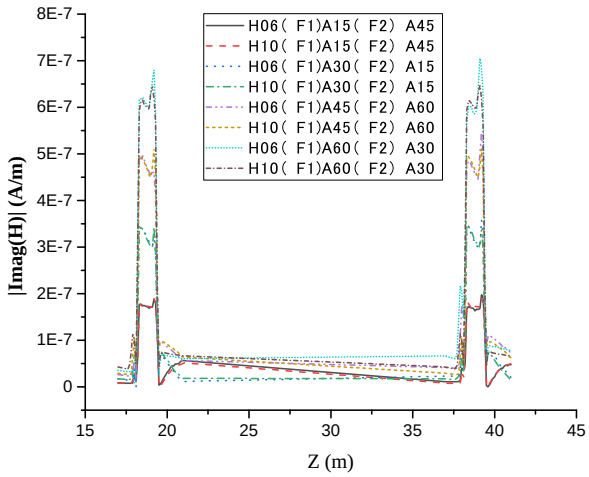

Fig. 8. The simulated results of multi-fracture system case with a constant length (The transmitting source plane perpendicular to the Z-axis).

3. An inversion method for electromagnetic monitoring of the propping fracture

3.1 Electromagnetic inversion and inverse problem analysis

The primary purpose of the inversion algorithm is to calibrate the parameters, i.e., fracture azimuth, length, and height, by fitting the simulation signal values to the observation signal values. The least-square method can be tentatively used to solve the inversion problems. However, due to the non-convergence problems caused by the solution of partial derivatives and parameters in different dimensions, it has no advantage. In recent studies, the DE algorithm has the advantage of simplicity, ease of improvement, and high adaptability which has been widely used in the inversion of electromagnetic signals.

3.2 Optimized inversion algorithm based on differential evolution method

DE algorithm performs better when the input variates are discrete data (Storn and Price, 1997). In general, the DE algorithm is preferable to a genetic algorithm (GA) and particle swarm optimization (PSO) (Vesterstrom and Thomsen, 2004). However, the DE algorithm tends to converge to local optimum and stop searching for the multi-peak problem of electromagnetic signals. In this regard, various improved DE algorithms have been proposed, such as DESAP (Teo, 2006), SADE (Qin and Suganthan, 2005), FADE (Brest et al., 2006), JDE (Liu and Lampinen, 2005), JADE (Zhang and Sanderson, 2007). The above algorithms adopt different variation strategies and adaptively change the control parameters in the DE to find the global optimal value. Chen et al. (2008) proposed an improved DE algorithm combining with a local search algorithm to accelerate the convergence and enhance the performance.

The improved differential algorithm for antenna optimization is applied to the inversion of propping fractures parameters according to the characteristics of electromagnetic signals (Wang and Zhang, 2009). As used in the field of electromagnetic fracture monitoring, the algorithm in this paper is called improved differential evolution algorithm (EMDE). Based on the JADE variation strategy, the difference between the population center and the individual is added to accelerate the convergence of the algorithm. A simplified selection strategy of the simulated annealing algorithm is used to enhance the convergence speed and the ability to find the global optimal value simultaneously.

The EMDE algorithm ameliorates the mutation and selection operators of the tranditional DE algorithm. The four operators of EMDE are described in detail below.

(1) Generating an initial random population

The independent variable of the objective function $O(\vec{\mathbf{M}})$ is a vector in D-dimensional continuous space R^D, $\vec{M} = (m_1, m_2, \cdots, m_D)$, its optimization goal is to make $O(\vec{\mathbf{M}})$ reach the minimum value. An initial population containing n individuals is set to distribute randomly and evenly in the solution space.

(2) Mutation operator

The individual $\vec{\mathbf{M}}_i^g$ in the generation g generates the offspring individual $\vec{\mathbf{V}}_i^g$ through mutation, the following mutation strategies are usually adopted (Wang and Zhang, 2009):

$$DE/rand/1: \vec{\mathbf{V}}_i^g = \vec{\mathbf{M}}_{r3}^g + F \cdot (\vec{\mathbf{M}}_{r1}^g - \vec{\mathbf{M}}_{r2}^g) \tag{10}$$

$$DE/best/1: \vec{\mathbf{V}}_i^g = \vec{\mathbf{M}}_{best}^g + F \cdot (\vec{\mathbf{M}}_{r1}^g - \vec{\mathbf{M}}_{r2}^g) \tag{11}$$

$$\begin{aligned} &DE/current-to-best/1: \\ &\vec{\mathbf{V}}_i^g = \vec{\mathbf{M}}_i^g + F \cdot (\vec{\mathbf{M}}_{best}^g - \vec{\mathbf{M}}_i^g) + F \cdot (\vec{\mathbf{M}}_{r1}^g - \vec{\mathbf{M}}_{r2}^g) \end{aligned} \tag{12}$$

$$\begin{aligned} &DE/best/2: \\ &\vec{\mathbf{V}}_i^g = \vec{\mathbf{M}}_{best}^g + F \cdot (\vec{\mathbf{M}}_{r1}^g - \vec{\mathbf{M}}_{r2}^g) + F \cdot (\vec{\mathbf{M}}_{r3}^g - \vec{\mathbf{M}}_{r4}^g) \end{aligned} \tag{13}$$

$$\begin{aligned} &DE/best/2: \\ &\vec{\mathbf{V}}_i^g = \vec{\mathbf{M}}_i^g + F \cdot (\vec{\mathbf{M}}_{r1}^g - \vec{\mathbf{M}}_{r2}^g) + F \cdot (\vec{\mathbf{M}}_{r3}^g - \vec{\mathbf{M}}_{r4}^g) \end{aligned} \tag{14}$$

$$\begin{aligned} &DE/current-to-best/2: \\ &\vec{\mathbf{V}}_i^g = \vec{\mathbf{M}}_{r5}^g + F \cdot (\vec{\mathbf{M}}_{best}^g - \vec{\mathbf{M}}_i^g) + F \cdot (\vec{\mathbf{M}}_{r1}^g - \vec{\mathbf{M}}_{r2}^g) \\ &\quad + F \cdot (\vec{\mathbf{M}}_{r3}^g - \vec{\mathbf{M}}_{r4}^g) \end{aligned} \tag{15}$$

where $\vec{\mathbf{M}}_{r1}^g$, $\vec{\mathbf{M}}_{r2}^g$, $\vec{\mathbf{M}}_{r3}^g$, $\vec{\mathbf{M}}_{r4}^g$, $\vec{\mathbf{M}}_{r5}^g$ is the random individual except $\vec{\mathbf{M}}_i^g$ in the population, respectively; $\vec{\mathbf{M}}_{best}^g$ is the individual which makes the objective function value minimum; F is the weight factor or mutation coefficient. Set its value interval as [0.2, 0.7].

When the individual $\vec{\mathbf{M}}_{best}^g$ of $DE/current-to-best/1$ is changed to $\vec{\mathbf{M}}_{best}^{g,p}$, $\vec{\mathbf{M}}_{best}^{g,p}$ is a random selection of the best p individuals in a population, $DE/current-to-p-best/1$ is proposed as:

$$\begin{aligned} &DE/current-to-p-best/1: \\ &\vec{\mathbf{V}}_i^g = \vec{\mathbf{M}}_i^g + F \cdot (\vec{\mathbf{M}}_{best}^{g,p} - \vec{\mathbf{M}}_i^g) + F \cdot (\vec{\mathbf{M}}_{r1}^g - \vec{\mathbf{M}}_{r2}^g) \end{aligned} \tag{16}$$

Combining with electromagnetic signals, n individuals in contemporary populations are divided into t subpopulations according to the fast clustering method in each iteration. The center of the subpopulation including individual $\vec{\mathbf{M}}_i^g$ is denoted as $\vec{\mathbf{M}}_C^g$, and the monomial with $\vec{\mathbf{M}}_C^g$ is added to the $DE/current-to-p-best/1$ mutation operator:

$$\begin{aligned} &DE/current-to-p-best/2: \\ &\vec{\mathbf{V}}_i^g = \vec{\mathbf{W}}_i^g + F \cdot (\vec{\mathbf{M}}_{\text{best}}^{g,p} - \vec{\mathbf{M}}_i^g) + F \cdot (\vec{\mathbf{M}}_{\text{C}}^g - \vec{\mathbf{M}}_i^g) \\ &\quad + F \cdot (\vec{\mathbf{M}}_{r1}^g - \vec{\mathbf{M}}_{r2}^g) \end{aligned} \tag{17}$$

Boundary constraints are added to the program to prevent the mutational individual from crossing the boundary. If the definitional domain of the parameter is known, the inversion efficiency can be promoted by adding constraints for optimization.

(3) Cross operator

Every $\vec{\mathbf{V}}_{j,i}^{g}$ in the $\vec{\mathbf{V}}_{i}^{g}$ proceeds the cross operation ($CR \in [0,1]$, $CR = 0.8$ in this paper):

$$\vec{\mathbf{W}}_{j,i}^{g} = \begin{cases} \vec{\mathbf{V}}_{j,i}^{g}, & if(rand_j[0,1] \le CR) \ or \ (j = rand(D)+1) \\ \vec{\mathbf{M}}_{j,i}^{g}, & else \end{cases} \tag{18}$$

Operates (2) and (3) are repeated n times to generate n initial individuals and n trained individuals.

(4) Selection operator

The traditional greedy selection operator of DE prone to resulting in the locally optimal solution, which can be avoided by the simulated annealing algorithm. Thereby, the EMDE selects the simplified simulated annealing (SA) as the selection operator.

$$\vec{\mathbf{M}}_{i}^{g+1} = \begin{cases} \vec{\mathbf{W}}, & if \ (O(\vec{\mathbf{W}}_{i}^{g}) < O(\vec{\mathbf{M}}_{i}^{g})) \ or \\ & (O(\vec{\mathbf{M}}_{i}^{g}) \ge O(\vec{\mathbf{M}}_{i}^{g}) \ \&\& \ rand(1) > P) \\ \vec{\mathbf{M}}_{i}^{g}, & otherwise \end{cases} \tag{19}$$

where,

$$P = \exp(-\Delta O/T) \tag{20}$$

When $P = 1$, Eq. (19) becomes the greedy selection operator; T is annealing control temperature, $T(g+1) = \alpha T(g)$, α is slightly less than 1. The setting of initial temperature T_0 is crucial for global optimal search. If is higher, the search of the global optima is easier, but it takes more time. On the other hand, the global optima may not be found, although it takes less time. Setting P as a constant could simplify the search algorithm.

Combining with the results of the forward simulation, the EMDE will be used for inversion optimization. The EMDE algorithm for electromagnetic fracture monitoring is in the appendix.

3.3 Objective function

Set the inversion objective function to minimize the variance of simulated and observed values:

$$O(\vec{\mathbf{M}}) = \sum_{j=1}^{NS} \left[w_j \sum_{i=1}^{n_j} \left(\frac{d_{\text{obs},i,j} - d_{\text{sim},i,j}}{d_{\text{obs},i,j}} \right)^2 \right] \tag{21}$$

where $O(\vec{\mathbf{M}})$ is the optimal objective function of inversion; $\vec{\mathbf{M}}$ is the fracture parameters to be corrected, including the azimuth, length and height of the fracture; NS is the number of downhole monitoring tool movement steps, i.e. assumed that one detection is carried out at each pause; n_j is the number of different signals received during a detection process; w_j is the crucial coefficient of the detection signal to the inversion results in j step; $d_{obs,i,j}$ is the observed (real) signal value; $d_{simu,i,j}$ is the simulated signal value obtained through the simulator.

The population number of each iteration is 10, while each population contains 10 individuals.

4. Inversion process and results

Through forward modeling, the monitoring signals are not sensitive to the positive and negative signs of the fracture azimuth (from the X-axis, the counterclockwise direction is positive, and the clockwise direction is negative). Therefore, it is necessary to obtain the signal when the transmitting source plane is perpendicular to the M-axis in the monitoring scanning process. In the inversion tests, it assumes that the fracture sign has been determined.

The observation data used in the inversion are the resultant magnetic field imaginary part signals. When the transmitting source plane is perpendicular to the Z-axis, the peak area signals include the information of the azimuth, length and height. The EMDE algorithm is employed to fit this set of observation data, and to observe the inversion effect.

The observation data only include the approximate interval when the monitoring tool scans the fracture and produces the peak area signal to reduce the computation during the inversion iteration. In the actual monitoring process, the fracture location is imprecise; the signals are recorded from the beginning to the end without interruption. The forward simulator is employed to generate the observation data, then the observation data set and the real data set tend to be the same through iteration, the objective function value is minimum, the simulated parameter is the real value.

In this paper, we have carried out inversion examples of 2 types: single fracture and double fractures, first of all, one-stage inversion of these two fracture structures is carried out. Every objective function value curve is plotted by the average data of twenty times running results.

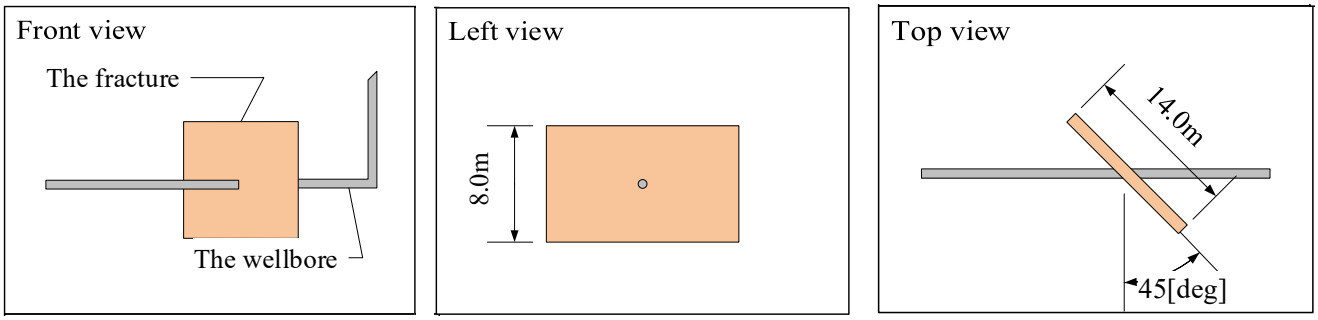

Fig. 9. The three views of the real single-fracture model.

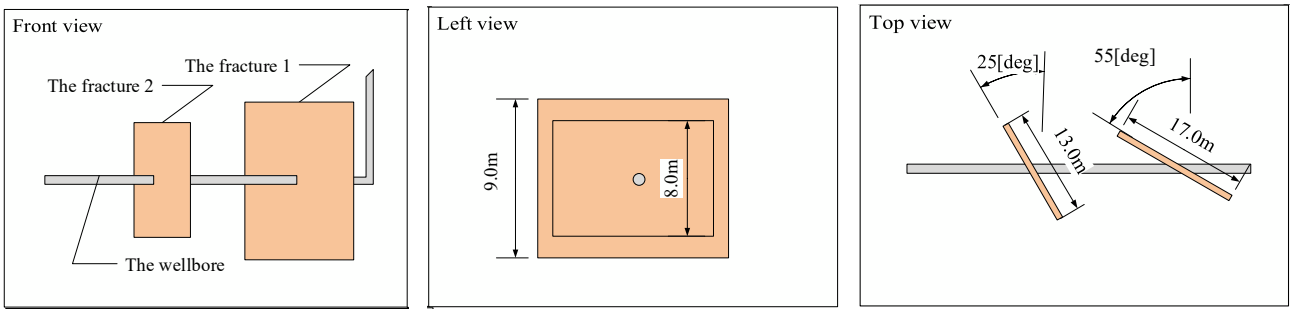

Fig. 11. The three views of the real double-fractures model.

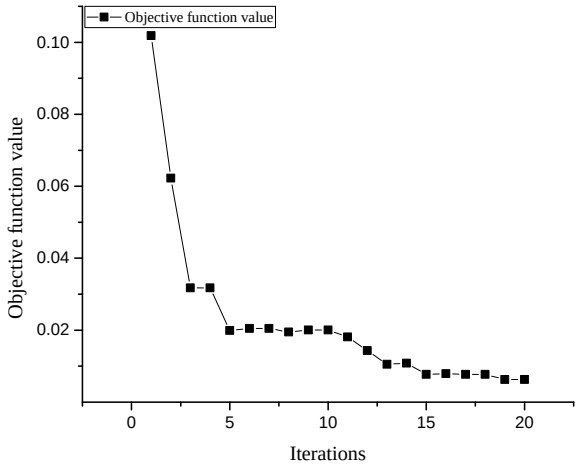

Fig. 10. The average objective function value curve of one-stage/single-fracture.

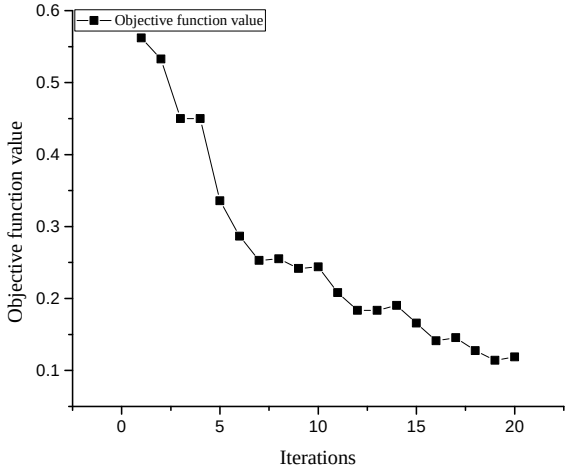

Fig. 12. The average objective function value of one-stage/double-fractures.

4.1 Case 1: One-stage inversion of single-fracture

Firstly, the single fracture model is simulated. The fracture parameters of the real model are given as: the azimuth is 45 [deg], the length is 14 m, the height is 8 m. The real fracture morphology is shown in Fig. 9.

After twenty generations of evolution (each generation contains ten individuals), the objective function value curve is shown in Fig. 10. The fracture parameters calculated by the one-stage inversion are: the azimuth is 48.96 [deg], the length is 12.04 m, the height is 9.85 m. After twenty inversion iterations of the EMDE, the error of the azimuth, length, and height all had a range of (5%-15%). It is found that the objective function value declines slowly, which is due to the multi-solution of the inversion process. If the value of the objective function decreases further after more iterative evolutions, there may still be a significant error.

4.2 Case 2: One-stage inversion of double-fractures

The model of double-fractures is inverted. The fracture parameters of the real model are given as: the first fracture's azimuth is 55 [deg], length is 17 m, height is 9 m. The second fracture's azimuth is 25 [deg], length is 13 m, height is 8 m. The real fracture morphology is shown in Fig. 11.

The objective function value curve is shown in Fig. 12. After twenty iterations of DE, the fracture parameters are calculated as: the first fracture's azimuth is 49.67 [deg], length is 14.63 m, height is 11.35 m. The second fracture's azimuth is 31.24 [deg], length is 11.82 m, height is 10.05 m.

The results of the one-stage inversion process demonstrate that its rate of convergence and accuracy of the results are both unsatisfactory. The error is higher than 5%, or even 20%. Thereby, the two-stages inversion process is purposed to promote the accuracy of the inversion results.

The first stage inversion sets the transmitting source plane perpendicular to the X-axis, in this position, the forward simulation finds signals are only sensitive to the azimuth of fractures, so that the azimuth can be accurately calculated. Due to the constraints of simulated forward results and the specific azimuth, the two-stages inversion method can be used to calculate the objective parameters more accurately; the difficulty and multi-solution of calculation are greatly reduced.

4.3 Case 3: Two-stages inversion of single-fracture

The established real model of case 3 is the same as that in case 1. Due to the inversion of the length and the height involving two parameters, more iterative evolution can get better

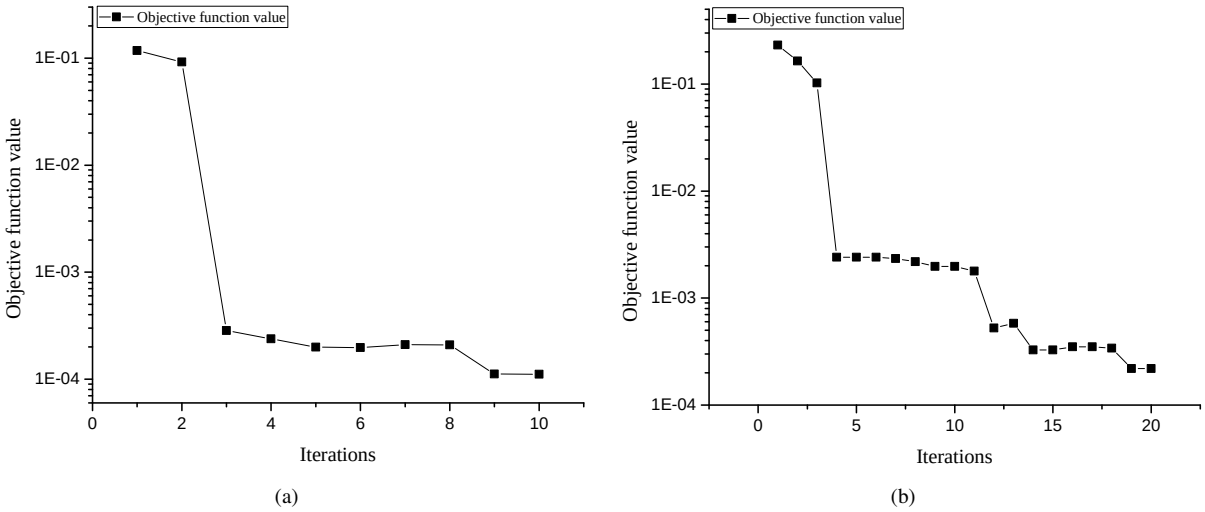

Fig. 13. The average objective function value curve of two-stages/single-fracture. (a) The first stage inversion (b) The second stage inversion.

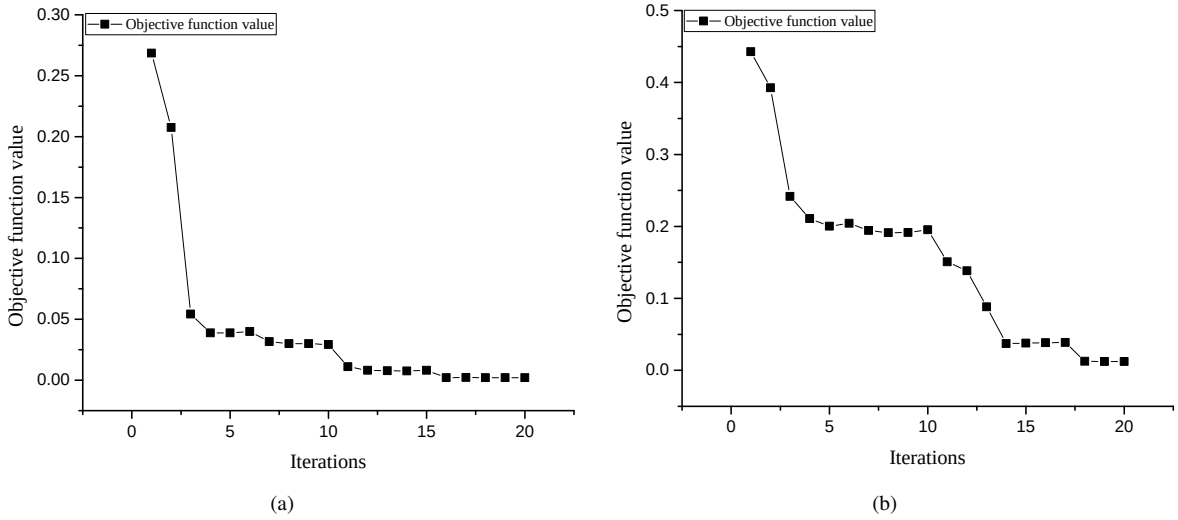

Fig. 14. The average objective function value curve of two-stages/single-fracture. (a) The first stage inversion (b) The second stage inversion.

results. Therefore, compared to the ten iterations in one-stage inversion, the inversion of the length and the height conducts twenty evolutionary iterations (each generation contains ten individuals), the objective function value curves of the two-stages inversion of single fracture are shown in Fig. 13.

The objective function value of the azimuth inversion decreases obviously in the third iteration, which is close to the optimal value. The objective function value of the length and the height inversion decreases obviously in the fourth iteration and in the 12th iteration, which is close to the optimal value. The inversion results are: the azimuth is 45.20 [deg], the length is 13.75 m, the height is 8.34 m.

It can be calculated that after two stages of EMDE inversion of the single fracture model, the errors of the azimuth, length, and height are all less than 5%. The accuracy of the two-stages inversion is higher than the one-stage single-fracture inversion. The reason is that, we only need to calculate azimuth in the first stage inversion. Therefore, the multi-solution of the algorithm is reduced, and the global search ability is improved. The law of the forward model and the accurate azimuth is used to constrain the second stage inversion, which reduces the uncertainty of the inverse problem.

4.4 Case 4: Two-stages inversion of double-fractures

The given real model is the same as that in case 2. After twenty iterations of evolution (the population number of each iteration is 10), the objective function value curves are shown in Fig. 14.

After twenty iterations of DE, the results are: the first fracture's azimuth is 54.46 [deg], length is 16.55 m, height is 9.32 m; The second fracture's azimuth is 25.37 [deg], length is 13.68 m, height is 7.65 m.

After two-stages EMDE inversion, the errors of the parameters, including the azimuth, length, and height of the two fractures, are all less than 5%. The two-stages inversion pro-

Table 2. The data of the inversion examples.

Case	Parameter	Set value (ture value)	Inversion revaluevalue (value)	Error, %
one-stage/single-fracture	azimuth, deg	45	48.96	8.09
	length, m	14	12.04	16.28
	height, m	8	9.85	18.78
one-stage/double-fractures	azimuth1, deg	55	49.67	10.73
	length1, m	17	14.63	16.2
	height1, m	9	11.35	20.7
	azimuth2, deg	25	31.24	19.97
	length2, m	13	11.82	16.2
	height2, m	8	10.05	20.4
two-stages/single-fracture	azimuth, deg	45	45.2	0.44
	length, m	14	13.75	1.82
	height, m	8	8.34	4.08
two-stages/double-fractures	azimuth1, deg	55	54.46	0.99
	length1, m	17	16.55	2.72
	height1, m	9	9.32	4.27
	azimuth2, deg	25	25.37	1.46
	length2, m	13	13.68	3.43
	height2, m	8	7.65	4.58

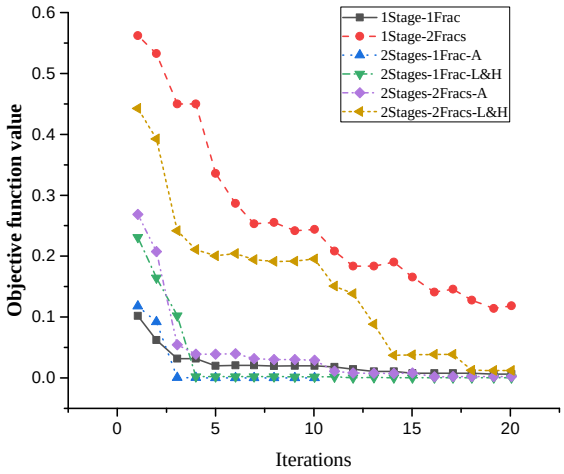

Fig. 15. The diagram of the average objective function value.

duces higher accuracy than one-stage inversion.

Compared to the one-stage inversion, the accuracy of both the single-fracture and the double-fractures results after the two-stage inversion is higher. It demonstrates that using the law of the forward model and the definite azimuth to constrain the inversion can well reduce the uncertainty of the inverse problem and significantly increase the reliability of the inversion results.

4.5 Inversion conclusion

The specific data for each case are summarized in Table 2.

Fig. 15 illustrates the value of the objective function falls faster in cases with fewer target parameters. For all cases, the value of the objective function has decreased significantly, even the global optima has been found in some cases within five iterations. Since the calculation of the length, the height and the azimuth are separated and constrained in the two-stages inversion, it can be clearly seen in Fig. 15 that the decline rate of the two-stages inversion is better compared to the one-stage inversion. According to Table 2, the former error is within the allowable range for field application (5%); It demonstrates that using the results of the forward simulation and the specific azimuth to constrain the inversion can effectively reduce the uncertainty of the inverse problem and significantly increase the reliability of the inversion results.

5. Conclusion

In this work, an EMDE is innovatively applied in the inversion process, based on an electromagnetic fracture monitoring method, and the EPV is accurately calculated.

A triaxial transmitting Tx-triaxial receiving Rx instrument is designed to transmit and receive electromagnetic signals. The sensitivity analysis found that selecting the imaginary part of the magnetic field signal as an observation signal is theoretically more advantageous. When the transmitting source plane is in a specific position, the relationship between the signals and a particular parameter is the most obvious. When the transmitting source plane is perpendicular to the Z-axis, the peak area of the signals is sensitive to the length and height, the value of the azimuth is corresponding to the transmitting source plane perpendicular to the X-axis, the sign of the azimuth is corresponding to the transmitting source plane

perpendicular to the M-axis. The forward simulation results can provide constraints for the inversion process, especially the two-stages inversion, to obtain more accurate inversion results.

The mutation and selection operator of the traditional DE algorithm are modified to make the DE algorithm more suitable to the fracture monitoring. In the inversion of the fracture parameters, we set up 4 cases to test the EMDE algorithm. One-stage and two-stage inversion strategies are proposed to calculate the parameters. In the second stage inversion is constrained by forward simulation and the first stage results. Findings indicate that the final result error of the two-stages inversion can be controlled within 5%. It is proved that the EMDE algorithm has high accuracy in the inversion of fracture parameters.

Acknowledgement

This work is supported by the National Natural Science Foundation of China under Grant 51722406, 51874335 and 51674280, the Shandong Provincial Natural Science Foundation under Grant JQ201808 and ZR2019JQ21, The Fundamental Research Funds for the Central Universities under Grant 18CX02097A, the Major Scientific and Technological Projects of CNPC under Grant ZD2019-183-008, the Science and Technology Support Plan for Youth Innovation of University in Shandong Province under Grant 2019KJH002 , the National Science and Technology Major Project of China under Grant 2016ZX05025001-006, 111 Project under Grant B08028.

Conflict of interest

The authors declare no competing interest.

References

Abubakar, A., Habashy. T.M. Three-dimensional single-well imaging of the multi-array triaxial induction logging data. Paper Presented at 2006 SEG Annual Meeting, New Orleans, Louisiana, 1-6 October, 2006.

Abubakar, A., Habashy, T.M., Druskin, V.L., et al. 2.5 D forward and inverse modeling for interpreting low-frequency electromagnetic measurements. Geophysics 2008, 73(4): F165-F177.

Alumbaugh, D.L., Wilt, M.J. A numerical sensitivity study of the three dimensional imaging from a single borehole. Petrophysics 2001, 42(1): 19-31.

Basu, S., Sharma, M.M. A new method for fracture diagnostics using low frequency electromagnetic induction. Paper SPE 168606 Presented at SPE Hydraulic Fracturing Technology Conference, The Woodlands, Texas, USA, 4-6 February, 2014.

Brest, J., Greiner, S., Boskovic, B., et al. Self-adapting control parameters in differential evolution: A comparative study on numerical benchmark problems. IEEE Trans. Evol. Comput. 2006, 10(6): 646-657.

Chen, Y., Yang, S., Nie, Z. The application of a modified differential evolution strategy to some array pattern synthesis problems. IEEE Trans. Antennas Propag. 2008, 56(7): 1919-1927.

Cipolla, C.L., Lolon, E., Mayerhofer, M.J., et al. The effect of proppant distribution and un-propped fracture conductivity on well performance in unconventional gas reservoirs. Paper SPE 119368 Presented at SPE Hydraulic Fracturing Technology Conference, The Woodlands, Texas, USA, 19-21 January, 2009.

Huang, Y., Boyle, K. Antennas: From theory to Practice. Chichester, UK, John Wiley & Sons Ltd, 2008.

LaBrecque, D., Brigham, R., Denison, J., et al. Remote imaging of proppants in hydraulic fracture networks using electromagnetic methods: Results of small-scale field experiments. Paper SPE 179170 Presented at SPE Hydraulic Fracturing Technology Conference, The Woodlands, Texas, USA, 9-11 February, 2016.

Li, M., Abubakar, A., Habashy, T.M. A three-dimensional model-based inversion algorithm for electromagnetic data inversion. Paper Presented at 2011 SEG Annual Meeting, San Antonio, Texas, USA, 18-23 September, 2011.

Liu, J., Abubakar, A., Habashy, T.M., et al. Nonlinear inversion approaches for cross-well electromagnetic data collected in cased-wells. Paper Presented at 2008 SEG Annual Meeting, Las Vegas, Nevada, USA, 9-14 November, 2008.

Liu, J., Lampinen, J. A fuzzy adaptive differential evolution algorithm. Soft Comput. 2005, 9(6): 448-462.

Mallan, R., Alumbaugh, D. The effects of anisotropy on 3D single-well imaging. Paper Presented at 2004 SEG Annual Meeting, Denver, Colorado, USA, 10-15 October, 2004.

Newman, G.A., Alumbaugh, D.L. Three-dimensional massively parallel electromagnetic inversion-I. Theory. Geophys. J. Int. 1997, 128(2): 345-354.

Palisch, T., Al-Tailji, W., Bartel, L., et al. Recent advancements in far-field proppant detection. Paper SPE 179161 Presented at SPE Hydraulic Fracturing Technology Conference, The Woodlands, Texas, USA, 9-11 February, 2016.

Qin, A., Suganthan, P.N. Self-adaptive differential evolution algorithm for numerical optimization. Paper Presented at IEEE Congress on Evolutionary Computation, Edinburgh, Scotland, UK, 2-5 Septenber, 2005.

Ruan, B. 1-D Optimazition inversion method for resistivity and IP sounding data. Journal of Guilin University of Technology 1999, (4): 321-325. (in Chinese)

Storn, R., Price, K. Differential evolutiona simple and efficient heuristic for global optimization over continuous spaces. J. Glob. Optim. 1997, 11(4): 341-359.

Symington, W.A., Kaminsky, R.D., Meurer, W.P., et al. ExxonMobil's Electrofrac^{TM} Process for In Situ Oil Shale Conversion, in Oil Shale: A Solution to the Liquid Fuel Dilemma, edited by O.I. Ogunsola, A.M. Hartstein, O.

Ogunsola, Oxford University Press, New York, pp. 185-216, 2010.

Teo, J. Exploring dynamic self-adaptive populations in differential evolution. Soft Comput. 2006, 10(8): 673-686.

Vesterstrom, J., Thomsen, R. A comparative study of differential evolution, particle swarm optimization, and evolutionary algorithms on numerical benchmark problems. Paper Presented at Proceedings of the 2004 Congress on Evolutionary Computation, Portland, Oregon, USA, 19-23 June, 2004.

Wang, A., Zhang, W. An improved differential evolution algorithm for antenna optimization. Chinese Journal of Radio Science 2009, 24(5): 808-812. (in Chinese)

Wang, Z., He, Z., Tang, B., et al. BSEM 3D inversion research and application case. Paper Presented at 2011 SEG Annual Meeting, San Antonio, Texas, USA, 18-23 September, 2011.

Zaslavsky, M., Druskin, V., Liu, J., et al. A three-dimensional multiplicative-regularized non-linear inversion algorithm for cross-well electromagnetic and controlled-source electromagnetic applications. Paper Presented at 2008 SEG Annual Meeting, Las Vegas, Nevada, USA, 9-14 November, 2008.

Zhang, J., Sanderson, A.C. JADE: Self-adaptive differential evolution with fast and reliable convergence performance. Paper Presented at IEEE Congress on Evolutionary Computation, Singapore, 25-28 September, 2007.

Zhang, K., Wei, W., Lv, Q., et al. The study of 2-D nonlinear conjugate gradients inversion of borehole-to-surface magnetotelluric. ACTA Geologica Sinica 2011, 85(5): 915-924. (in Chinese)

Zhang, L., Qi, J., Li, L., et al. A forward modeling method based on electromagnetic theory to measure the parameters of hydraulic fracture. Fuel 2019, 251: 466-473.

Appendix

Algorithm1: The EMDE algorithm for electromagnetic fracture monitoring

INPUT: Fractures to be observed; Horizontal well length; Number of fractures *Nm*; Instrument moving step; Objective function $O(\vec{\mathbf{M}}_i^g)$.

OUTPUT: The solution of the g th iteration.

Initialize the population M.

For i = 1; *Num*_Pop % *Num*_Pop is the number of individuals in a population;

Calculate the objective function of the i th individual $O(\vec{\mathbf{M}}_i^g)$;

End

For g = 1:n % g is the iteration number, n is the maximum number of iterations;

Identify the best individual $\vec{\mathbf{M}}_{best}^{g,p}$ of the p better individuals in the population;

Calculate the center of the current population $\vec{\mathbf{M}}_C^g$;

For i = 1: *Num*_Pop

Variable coefficient $F \leftarrow [0.2, 0.7]$;

randomly pick two individuals $\vec{\mathbf{M}}_{r1}^g$, $\vec{\mathbf{M}}_{r2}^g$, $(\vec{\mathbf{M}}_{r1}^g \neq \vec{\mathbf{M}}_i^g, \vec{\mathbf{M}}_{r2}^g \neq \vec{\mathbf{M}}_i^g)$;

generate the intermediate *rand*_1 and *best*_1;

mutate according to Eq. (17), get the mutation individual $\vec{\mathbf{V}}_i^g$ of $\vec{\mathbf{M}}_i^g$;

cross each $\vec{\mathbf{V}}_{j,i}^g$ in $\vec{\mathbf{V}}_i^g$, $CR \leftarrow 0.8$, D is the dimension of R;

for j = 1:i

if $(rand_j[0,1] \leq CR)$ *or* $(j = rand(D) + 1)$

new individual $\vec{\mathbf{W}}_{j,i}^g = \vec{\mathbf{V}}_{j,i}^g$

else $\vec{\mathbf{W}}_{j,i}^g = \vec{\mathbf{M}}_{j,i}^g$

calculate the objective function value $O(\vec{\mathbf{V}}_{j,i}^g)$ of $\vec{\mathbf{V}}_{j,i}^g$

if $(O(\vec{\mathbf{W}}_i^g) < O(\vec{\mathbf{M}}_i^g))$ *or* $(O(\vec{\mathbf{W}}_i^g) \geq \vec{\mathbf{M}}_i^g)$ && $rand(1) > P)$ % P is defined in Eq. (20)

$\vec{\mathbf{M}}_i^{g+1} = \vec{\mathbf{W}}_i^g$

Else

$\vec{\mathbf{M}}_i^{g+1} = \vec{\mathbf{M}}_i^g$

End

End

End